International Soil and Water Conservation Research xxx (xxxx) xxx

Contents lists available at ScienceDirect

International Soil and Water Conservation Research

journal homepage: www.elsevier.com/locate/iswcr

Original Research Article

Unveiling water dynamics at soil-plant level using geophysical imaging under sustainable farming practices in Mediterranean citrus groves

Daniela Vanella [a,*], Ulrike Werban [b], Giuseppe Longo-Minnolo [a], Serena Guarrera [a], Marco Pohle [b], Simona Consoli [a]

[a] Dipartimento di Agricoltura, Alimentazione e Ambiente (Di3A), Università degli Studi di Catania, Via S. Sofia, 100, Catania, 95123, Italy
[b] Monitoring & Exploration Technologies, Helmholtz Centre for Environmental Research - UFZ, Permoserstr. 15, 04318, Leipzig, Germany

ARTICLE INFO

Article history:
Received 4 September 2025
Received in revised form
10 March 2026
Accepted 5 April 2026
Available online xxx

Keywords:
Agrogeophysics
Soil water motion
Conservation agricultural practices
Soil and crop water status

ABSTRACT

This study assesses the combined effects of different water regimes (full irrigation−FI *versus* regulated deficit irrigation−RDI) and soil management practices (with/without the use of organic soil mulching−OM) on spatiotemporal patterns of soil water content (SWC) (case study 1) and soil-plant-water dynamics (case study 2) in a citrus orchard located in Mediterranean semi-arid climate. Repeated electrical resistivity tomography (ERT) surveys were performed adopting dipole-dipole electrode arrays within two periods of the irrigation seasons 2022-2023 (both at case study 1 and 2), before and during irrigation events. Electromagnetic induction (EMI) technique was applied at case study 2 under dry conditions (no irrigation) in order to complement by spatial continuous geophysical coverage. Electrical resistivity (ER)-dependent parameters (e.g., SWC; soil temperature, T_{soil}) and continuous tree water status measurements, i.e., crop transpiration (T_{SF}) and trunk water potential (TWP), were also acquired. At case study 1, the OM reduced the ER and increased SWC by 14 % under RDI (p-value = 0.00), suggesting lower soil evaporation and enhanced moisture retention. Both ERT and EMI showed lower ER and higher apparent conductivity under mulched soils compared to bare soils at case study 2. As consequence of irrigation, ER was increased by OM up to 14 %, resulting in an inverted trend of SWC and T_{soil} in contrast to the observed T_{SF} and TWP. In conclusion, the use of geophysical imaging and complementary measurements offered practical insights by contributing to improve our understanding on key soil-hydrology related processes and soil-plant water dynamics in citrus groves under OM application.

1. Introduction

Understanding the effects of adopting sustainable soil and water management practices (SWMPs) on the soil system is pivotal for ensuring the responsible use of soil and water resources, and overall for targeting a more sustainable agriculture according to the Sustainable Development Goals and circular economy paradigms (Al-Shammary et al., 2024; Han & Niles, 2023; Löbmann et al., 2022).

Within this context, geophysics provides an extensive range of methods, based on electrical resistivity tomography (ERT) and electromagnetic techniques (EMI), for inferring soil properties and state variables, including soil water content (SWC), across a wider range of spatial and temporal scales (Binley & Slater, 2020). In this sense, electrical resistivity (ER), or its reciprocal (electrical conductivity, EC), is commonly inverted or derived to describe dynamics relevant to agricultural management (Allred et al., 2008; Becker et al., 2025; Romero-Ruiz et al., 2024), as it is highly sensitive to SWC. Notably, time-lapse ERT approaches have enabled to track the variations of soil state variables, e.g., due to root-water

* Corresponding author.
E-mail address: daniela.vanella@unict.it (D. Vanella).

Peer review under the responsibility of International Research and Training Center on Erosion and Sedimentation, the China Water and Power Press, and China Institute of Water Resources and Hydropower Research.

https://doi.org/10.1016/j.iswcr.2026.100660

Please cite this article as: D. Vanella, U. Werban, G. Longo-Minnolo *et al.*, Unveiling water dynamics at soil-plant level using geophysical imaging under sustainable farming practices in Mediterranean citrus groves, International Soil and Water Conservation Research, https://doi.org/10.1016/j.iswcr.2026.100660

uptake (RWU) process, under heterogeneous agro-systems (Cassiani et al., 2015; Blanchy et al., 2020; Vanella et al., 2018, 2023). Recent studies have been focussed on identifying the subsurface water flow pathways under precision irrigation scenarios in perennial crops (e.g., Araya Vargas et al., 2021; Scudiero et al., 2024; Vanella et al., 2021, 2022). At the same time, the use of EMI technique has been demonstrated to be effective in providing insights on the subsurface distribution of the main soil variables, such as grain size and SWC (von Suchodoletz et al., 2022). Nowadays, this method has been exploited for assessing the spatio-temporal variability of soil features for identifying suitable agricultural management zones (Pathirana et al., 2023) and for guiding the implementation of hydrological modelling (Peruzzo et al., 2025). All the above-mentioned geophysical applications represent practical examples of the so-called agrogeophysics discipline that recently has opened up innovative possibilities to underpin complex processes that characterize the soil-plant *continuum* of interest for field management purposes (Becker et al., 2025; Garrè et al., 2021; Romero-Ruiz et al., 2024).

Despite SWMPs are increasingly promoted as eco-schemes in perennial cropping systems under the recent Common Agricultural Policy (CAP) 2023–2027 framework (European Commission, 2023; Regulation (EU) 2021), the understanding of spatiotemporal soil–plant water dynamics under these sustainable practices is still limited. Few studies have identified the effects of SWMPs, including the use of soil organic mulching (OM) and/or amendments, on the soil-plant interface using ERT-based approaches applied in open field conditions (Carrera et al., 2022; Chen et al., 2019; Kisekka and al., 2024). For instance, Chen et al. (2019) found that the ERT-derived SWC, induced by rainfall and soil drying events, was dissimilar under both mulched and bare strips, resulting in a high degree of irregularity for a maize cultivation. Kisekka et al. (2024) assessed the beneficial effects on RWU and soil infiltration rates of almond trees managed with organic matter amendments using time-lapse ERT-based observations. Carrera et al. (2022) have deepened the responses of agronomic management systems on soil properties using both ERT and EMI techniques, resulting in a strong variability of tilled soils in comparison to conservative agricultural practices. Moreover, no studies have investigated the soil-plant response to SWMPs in citrus groves under Mediterranean climate conditions adopting ERT and EMI imaging. Consequently, how OM application and DI regimes jointly influence soil hydrology-related features and soil–plant water dynamics at the field scale remains poorly understood. Based on this knowledge gap, the hypothesis that was behind this study is that the adoption of sustainable SWMPs, namely OM application and DI regimes, may differently affect soil hydrology-related features, by reducing soil evaporation and enhancing moisture retention, as well as soil-plant response by delaying or attenuating the soil and crop water status. Accordingly, the overall framework of this study was to investigate the spatially response of soil–plant system to sustainable SWMPs in orange orchards using a novel approach based on ERT, EMI and multiple complementary measurements, related to ER-dependent parameters, and soil and crop water status measurements. The specific objectives (SO) of the study were to: (1) explore the combined effects of water regime and soil management on inferred soil hydrology-related features at the soil-plant interface (case study 1, SO1), and (2) assess the response on soil-plant-water dynamics under bare and mulched soils subjected to RDI (case study 2, SO2).

2. Methodological approach

2.1. Study site description

The methodological approach presented in this study was performed in an adult orange orchard [*Citrus sinensis* (L) Osbeck] 'Tarocco Sciara' C1882 on Carrizo citrange rootstock [*Poncirus trifoliata* (L.) Raf. × *C. sinensis* (L.) Osbeck] located in Eastern Sicily (Lentini, 37°20′12.65″ N, 14°53′33.04″ E, WGS84) under semi-arid Mediterranean climate and managed by the Italian Council for Agricultural Research and Agricultural Economics Analyses (CREA-OFA, Acireale) (Fig. 1).

Sustainable SWMPs were applied during the period 2021–2023 (Guarrera et al., 2024; Pappalardo et al., 2023; Vanella et al., 2025), consisting in the combination of different water regimes, i.e., full irrigation (FI) and regulated deficit irrigation (RDI) and the use of OM, as soil cover, in comparison to the adoption of bare soil conditions. In detail, the OM layer was posed on the soil surface every year, before the beginning of each irrigation season and it was made of crop residues from citrus orchard pruning and intercrop weed residuals. The combination of the above-mentioned experimental factors (i.e., water regime and soil management) resulted in the following SWMPs: (1) a FI regime, with irrigation rate equals to 100 % of the crop evapotranspiration (ET_c) under bare soil conditions (FI-Bare); (2) a FI regime under OM conditions (FI-Mulch); (3) a RDI regime, irrigated at 100 % ET_c, except for the II phenological stage (i.e., fruit growth phase), with irrigation rate equals to 50 % of ET_c in bare soil conditions (RDI-Bare); and (4) a RDI regime under OM conditions (RDI-Mulch). Water deficit under RDI was consistent and applied to the same fruit growth stage each year, and, specifically, from the days of the year (DOYs) 214 and 212, respectively, in 2022 and 2023, until the end of each irrigation season (DOYs 259 and 272, respectively).

Note that irrigation uniformity was checked during the geophysical campaigns (Section 2.2), indicating an overall good performance of the adopted drip irrigation systems. Further details on the adopted drip irrigation scheme and crop water requirement (ET_c) calculation are reported in Pappalardo et al. (2023), Guarrera et al. (2024) and Vanella et al. (2025). In addition, during the ERT surveys, the EC of irrigation water samples was measured, using a portable conductivity meter (HD2106.2, delta OHM, Italy), indicating average values of 1.97 ± 0.19 mS m^{-1}.

According to the United States Department of Agriculture (USDA) soil classification, the soil at the study site has a sandy loam/sandy clay loam texture (i.e., sand 56.86 %, silt 23.94 %, clay 19.20 % including the soil organic matter), with organic matter equal to 2.53 % (Guarrera et al., 2024). Additional details on the main soil physical-chemical variables under the SWMPs of interest are reported in Vanella et al. (2025). The full details on the soil hydraulic characterization conducted at the study site under the explored SWMPs of interest are given in Section 2.4.

Geophysical imaging methods, including ERT and EMI imaging, were applied at the SWMPs of interest (named in the following as case study 1 and 2) as reported in the sub-sections 2.2.1 and 2.2.2, respectively, in reference to the specific objectives of the study as given in Fig. 2.

An overview of the ERT layout arrays applied at case study 1 and 2 is depicted in Fig. 1, together with the localizations of the ancillary sensors adopted for continuously monitoring the main soil variables, i.e., SWC and soil temperature (T_{soil}) probes, and the

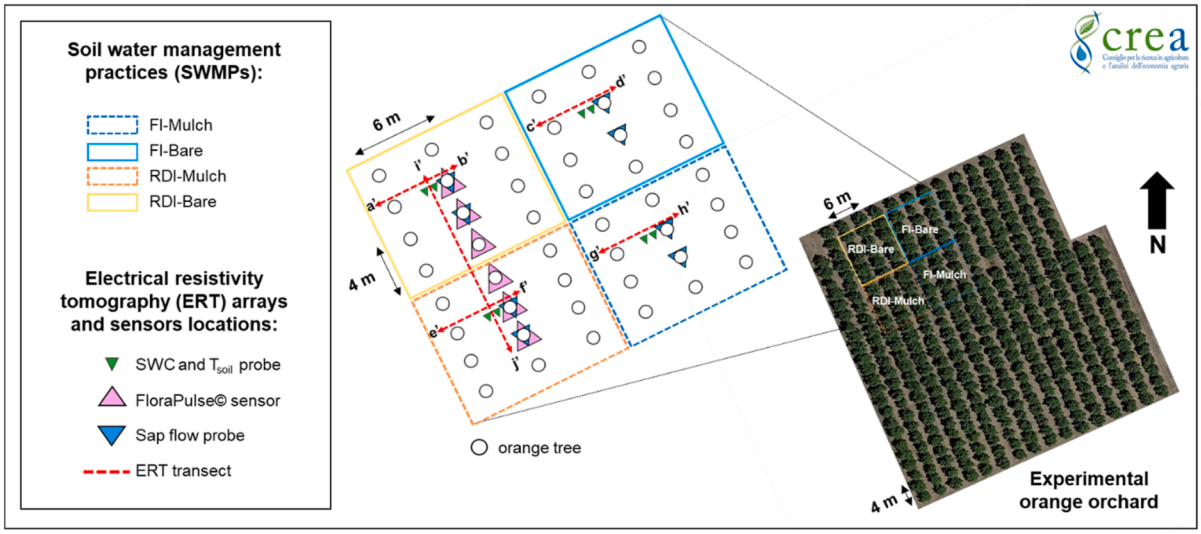

Fig. 1. Overview of the electrical resistivity tomography (ERT) linear arrays and point-based sensors locations at case studies 1 and 2. The terms FI-Mulch, FI-Bare, RDI-Mulch and RDI-Bare refer to the soil water management practices of interest (see description in Section 2.1). Electromagnetic measurements were performed across the full extent of the study area.

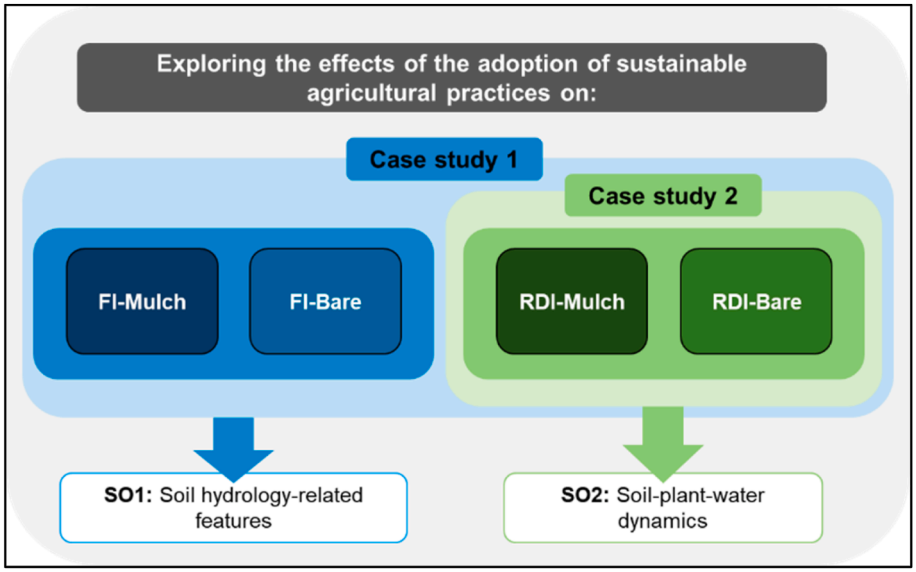

Fig. 2. Conceptual flowchart of the methodological framework, highlighting the specific objectives (SO) addressed in case study 1 (SO1) and case study 2 (SO2).

tree water status, i.e., sap flow and FloraPulse© sensors, for estimating the trunk water potential (TWP) and crop transpiration fluxes (T_{SF}), respectively, (refer to description in Section 2.3).

2.2. Geophysical monitoring at the case studies

2.2.1. ERT surveys: data collection, accuracy assessment and inversion

The ERT datasets, including both direct and reciprocal quadrupoles, i.e. by swapping potential with current electrodes for each ERT acquisition, were collected using a 10 channel Syscal Pro georesistivimeter (IRIS Instruments, Orleans, France). Due to its intrinsic strength and sensitivity in solving ER lateral changes compared to other arrays (e.g., Wenner-Schlumberger), which are better for vertically extended structures, a dipole-dipole electrode configuration was used (Samouëlian et al., 2005) at case study 1 and 2 (Fig. 1). Each collected ERT dataset was made of 5097 readings, with average acquisition timing of 20–30 min (Tables 1 and 2). The electrode galvanic contacts were checked before each ERT dataset acquisition.

At case study 1, a total number of 40 ERT datasets were acquired, covering all the SWMPs under study (i.e., FI-Bare, FI-Mulch, RDI-Bare, RDI-Mulch; Fig. 1 and Section 2.1). Specifically, linear ERT arrays, made of 72 surface electrodes, spaced 0.15 m each other and buried into the soil surface for 1/3 of their length (~20 cm), were arranged perpendicular to the tree lines, covering two trees for a total length of 10.65 m (Fig. 1) per treatment. With this electrode arrays, 2 or 1 emitters for tree (with a flow rate of 4 L h^{-1}) were intercepted in FI and RDI (at 50 % of FI) regimes, respectively, under both bare and mulched soils. Multiple ERT linear surveys (refer to ERT transects a'-b'; c'-d'; e'-f'; g'-h' in Fig. 1) were conducted in two separate periods of the irrigation season 2022, referring to the

Table 1
Scheduling of the electrical resistivity tomography (ERT) surveys conducted at case study 1 on July and September, 2022. The time hh:mm denotes the local time. The terms FI-Mulch, FI-Bare, RDI-Mulch and RDI-Bare refer to the soil water management practices of interest (see description in Section 2.1).

Soil water management practices	Date	ERT time-step	Start time (hh. mm)	End time (hh. mm)	Irrigation phase
RDI-Bare	06/07/2022	time 0	09:28	09:55	No
		time 1	10:02	10:28	During irrigation
		time 2	10:32	10:56	
		time 3	11:04	11:31	
		time 4	11:36	12:00	
RDI-Mulch	08/07/2022	time 0	09:42	10:10	No
		time 1	10:20	10:47	During irrigation
		time 2	10:51	11:16	
		time 3	11:22	11:48	
		time 4	11:52	12:19	
FI-Bare	11/07/2022	time 0	07:47	08:15	No
		time 1	08:18	08:45	During irrigation
		time 2	08:48	09:15	
		time 3	09:18	09:44	
		time 4	09:47	10:15	
FI-Mulch	13/07/2022	time 0	09:12	09:39	No
		time 1	09:55	10:22	During irrigation
		time 2	10:26	10:53	
		time 3	10:57	11:23	
		time 4	11:26	11:52	
RDI-Bare	16/09/2022	time 0	10:04	10:37	No
		time 1	10:42	11:11	During irrigation
		time 2	11:13	11:44	
		time 3	11:45	12:12	
		time 4	12:13	12:32	
	21/09/2022	time 0	10:26	10:58	No
		time 1	11:07	11:35	During irrigation
		time 2	11:36	12:05	
		time 3	12:09	12:35	
		time 4	12:38	13:08	
FI-Bare	19/09/2022	time 0	10:05	10:39	No
		time 1	10:44	11:05	During irrigation
		time 2	11:22	11:51	
		time 3	11:52	12:20	
		time 4	12:23	12:49	
FI-Mulch	28/09/2022	time 0	10:12	10:32	No
		time 1	10:55	11:25	During irrigation
		time 2	11:27	11:57	
		time 3	11:59	12:28	
		time 4	12:34	13:03	

Table 2
Scheduling of the electrical resistivity tomography (ERT) surveys conducted at case study 2 on June and August, 2023. The time hh:mm denotes the local time. The terms FI-Mulch, FI-Bare, RDI-Mulch and RDI-Bare refer to the soil water management practices of interest (see description in Section 2.1).

Date	ERT time-step	Start time (hh:mm)	End time (hh:mm)	Irrigation phase
29/06/2023	time 0	12:10	12:30	No
	time 1	12:46	13:06	
	time 2	13:22	13:42	
04/08/2024	time 0	10:00	10:20	During irrigation
	time 1	10:30	10:50	
	time 2	11:00	11:20	
	time 3	11:30	11:50	
	time 4	12:00	12:20	

beginning and the end of the season, respectively (i.e., July and September, Table 1). Additionally, short-term ERT repetitions were performed, for each time-period, within the irrigation cycles on both July and September (Table 1). Thus, the experimental time-lapse ERT monitoring protocol performed at case study 1 consisted in: (1) acquiring a first dataset before the beginning of the irrigation event (time 0, in Table 1) on July and September, and (2) performing a number of ERT repetitions (from time 1 to time 4, in Table 1) during single irrigation phases (each lasted about 2.5 h).

At case study 2, ERT campaigns were designed for exploring the soil-plant water exchanges at the RDI regime under both bare and organic mulched soil conditions (i.e., RDI-Bare and RDI-Mulch, refer to ERT transect i'-j' in Fig. 1). For this purpose, a linear array, made of 72 surface electrode, spaced 0.4 m each other, was placed in parallel to the tree rows (and the surface drip irrigation lines), covering the SWMPs of interest for a total length of 28.4 m. Note that at least 20 emitters (with a flow rate of 4 L h^{-1}) and three trees were covered by each ERT survey under RDI-Bare and RDI-

Mulch conditions, respectively. In detail, repeated ERT acquisitions were performed at the beginning and in the middle phase of the irrigation season 2023, under drying and wetting conditions, respectively (Table 2). In particular, three datasets were acquired on June 29th under dry conditions (time 0–2); whereas, on August 4th one dataset was collected before the beginning of the irrigation phase (time 0) and four datasets (from time 1 to time 4) were recorded within an irrigation event (lasted about 2.5 h), as reported in Table 2.

Several sources of uncertainties may affect the ERT measurements over time, such as, data acquisition uncertainty, external factors and model errors (Binley, 2015). In this study, data acquisition uncertainty due to improper spacing of the electrodes can be excluded, since surface electrodes were always left in place at same location, both at case studies 1–2 during the time-lapse ERT measurements (Fig. 1). Commonly, to avoid the effects of external factors on ER, it is recommended to quantify case-by-case ER-dependent variables (including soil properties/state variables, and roots distribution) and ancillary data (refer to sections 2.3 and 2.4) for accurately interpreting the temporal ER behaviour at the soil-plant level. During the ERT readings, environmental factors, such as T_{soil} and irrigation water salinity, showed limited variability, as all ERT datasets were acquired within the same daily time window (Tables 1 and 2) and during the same irrigation season, coinciding with the summer period in both case study 1 (July and September 2022) and case study 2 (June and August 2023). In general, T_{soil} correction in ERT datasets may be relevant when considering seasonal long-term ER variations, since ER is temperature dependent (Samouëlian et al., 2005). However, our methodological approach minimized temperature-induced variability, as T_{soil} remained consistently high and relatively uniform across the study area, with average variations not exceeding 2 °C (Figs. 4 and 9). Given this limited T_{soil} variability, the expected thermal effect (theoretical maximum ~4 %; Friedman, 2005; Nijland et al., 2010) can be regarded as a systematic background influence and, therefore, did not affect the relative spatial contrasts used to assess treatment differences, which were primarily attributed to SWC dynamics. Similarly, the EC of irrigation water was quite stable during the ERT surveys during both the irrigation seasons 2022–2023; thus, salinity should not affect the sensitivity of the ERT measurements, being ER mostly induced by preferential flow rather than salinity (Brindt et al., 2019). Note that the influence of roots that in some cases may be consistent, i.e., for herbaceous crops (Rao et al., 2019), in this study was neglected since no short-term changes of root distribution are expected for adult orange trees. Due to the high-accuracy of the ERT data assessment, herein the SWC variability was inferred on the basis of the observed ER heterogeneity, due to soil hydrological and irrigation processes, being that the absolute translation of ER into SWC prone to additional uncertainty (is not deepened in this study; e.g. Calamita et al., 2017; Tso et al., 2019).

Data quality control steps, including data filtering and error modelling phases, were performed for each ERT dataset collected at case studies 1 and 2 in order to determine the weights used to tie the inversion process. In particular, measurement uncertainty was computed on the basis of the reciprocal errors according to the procedure proposed by Slater et al. (2000), i.e., removing the quadrupoles with reciprocity error above 10 % and measurements that did not have a reciprocal pair (corresponding in average to 20 % of the original dataset).

Then, the ERT datasets were then inverted in absolute (initial condition, i.e., no irrigation, Tables 1 and 2) and relative modes. Bi-dimensional (2-D) forward and inverse models were executed using the freeware R2 code (http://www.es.lancs.ac.uk/people/amb/Freeware/R2/R2.htm) that implements a finite element based model developed by Binley and Kemna (2005) for solving direct current ER problems. *Ad hoc* unstructured triangular meshes were generated using the Gmesh meshing code in order to get more efficient the model computation (Geuzaine & Remacle, 2009). For each ERT inversion, the normal regularisation mode was applied. To update the weights as the inversion progresses, the routine implemented into the R2 code was applied. Note that the smoothing parameters (*alpha*) were searched for each iteration. The parameter (*alpha_aniso*) that is the anisotropy of the smoothing factor was set to 1 for normal (isotropic) regularisation.

The ratio time-lapse inversion approach was applied for retrieving the ER changes at the different temporal steps explored during the irrigation phases in comparison to the initial condition (i.e., no irrigation, Tables 1 and 2), for the applied SWMPs during the irrigation seasons 2022–2023. Specifically, the resistance ratio was calculated, and then inverted, on the basis of the common quadrupoles filtered among the ERT datasets acquired in time-lapse mode, as follows:

$$d_r = \frac{d_t}{d_0} F(\sigma_{ohm}) \quad (1)$$

where, d_r is the resistance ratio (Ω), d_t and d_0 (Ω) are the resistance dataset collected at selected time periods (t_1–t_7) and at the initial condition (t_0), and $F(\sigma_{ohm})$ is the resistance value (Ω) obtained by running the forward model for a fixed ER value (i.e., 100 Ω m).

According to Eq. (1), the ratio time-lapse inversion approach permitted to recognize the ER changes (%) in comparison to the initial condition (no irrigation, Tables 1 and 2) and, thus, to infer wetting or drying soil patterns, e.g., resulting in a decrease or increase in ER compared to the initial dataset (Binley et al., 2015). The main advantage of the ratio time-lapse inversion approach is its ability to suppress systematic errors and noise, resulting in a sharper and more accurate image of changes over time. For further methodological details refer to Vanella et al. (2018, 2021, 2022, 2023). The reconstruction of the 2-D ERT tomograms was performed using the ParaView software (v. 4.4.0).

Non-parametric statistical tests based on Kruskal–Wallis analysis was applied to formally assess variations in ER in time and as function of the adopted SWMPs (water regime and/or soil management) both at case study 1 and 2 using Statistix software (v.9.0, Analytical Software, Miller Landing Rd Tallahassee, FL), p-value < 0.05 was considered to indicate statistical significance.

2.2.2. EMI data collection and processing steps

A near-surface based EMI survey was employed to map the spatial distribution of the soil subsurface at the entire orange orchard level (0.75 ha) under dry conditions (no irrigation) on June 29th, 2023 (Fig. 1), in conjunction with the ERT measurements acquired at case study 2 (Table 2), before noon under constant sunny weather conditions.

An EMI sensor (CMD-Mini-Explorer; GF Instruments s.r.o., Brno, Czech Republic) was employed, enabling simultaneous multi-depth exploration using three different intercoil spacing, i.e., 0.32 m, 0.71 m and 1.18 m and two dipole orientations, i.e., vertical and horizontal mode. The EMI sensor measured the apparent electrical conductivity (ECa, mS m^{-1}) and data were sampled at a rate of 5 records per second. Note that EMI sensor was directly connected to a D-GPS (Hemisphere A43 Antenna) for precise positioning purposes.

To achieve effective penetration depths of 0.5 m, 1.0 m, and 1.8 m, respectively, the vertical dipole (VDP) was set at coil spacing of 0.32 m (VDP1), 0.71 m (VDP2), and 1.18 m (VDP3), where 75 % of the cumulative sensitivity was achieved (McNeill, 1980). To ensure data quality, cross-line measurements and reference lines were

employed to identify and correct for any drifts and offsets. The reference lines showed minor offsets (VDP1 = 2 mS m^{-1}, VDP2 = 0.2 mS m^{-1}, VDP3 = 1.8 mS m^{-1}), which were corrected along with single outliers. Thus, the point-based ECa values were spatially interpolated onto a 2 m × 2 m grid using the ordinary kriging method (block kriging). The semivariograms were modeled using a combination of spherical and linear functions.

2.3. Soil and tree water status monitoring

Ancillary data on the soil and tree water status was continuously acquired at both case studies 1–2 (Fig. 1). The SWC and T_{soil} were monitored at the ERT transects a'-b'; c'-d'; e'-f'; g'-h' through the use of eight TEROS-12 sensors (Meter Group, Washington-USA) installed at a depth of 0-30 cm and located at two distances from the tree trunks, i.e., 0.35 m and 0.75 m, respectively, in correspondence of sample orange trees, as given in Fig. 1. Sensors were calibrated using a factory process that minimizes sensor-to-sensor variability. Preliminary checks against factory standards were performed on undisturbed soil samples by gravimetric methods. Semi-hourly SWC and T_{soil} records were acquired using a CR1000 datalogger (Campbell Scientific, USA) and, then, aggregated at the daily scale. Note that T_{soil} changes were monitored to correct for their effect on ER, if necessary.

The tree water status was tracked using plant-based techniques that implied the adoption of microtensiometer sensors and sap flow probes. More in detail, at the ERT transect i'-j' (Fig. 1), six microtensiometers (FloraPulse©, Davis, CA, USA) were embedded into the woody tissues of sample orange trees under RDI-Bare and RDI-Mulch for continuous monitoring the TWP. The microtensiometer sensors were installed on the western side of the tree trunks, at 60 cm from the soil surface, according to the procedure described by the manufacturer (https://florapulse.com/resources/). Semi-hourly data was recorded and managed by a datalogger (CR1000, Campbell Scientific, USA). In addition, sap flow sensors (Tranzflo NZ Ltd, New Zeland), made of a linear heater and two temperature probes, radially inserted into the trunks of two sample orange trees under the SWMPs of interest (Fig. 1), were used for computing the sap flow fluxes according to the compensation heat-pulse technique described by Swanson and Whitfield (1981). Semi-hourly data was collected using a CR1000 datalogger (Campbell Scientific, USA) and, then, the T_{SF} were estimated at the tree level according to the procedure reported in Consoli et al. (2017).

2.4. Soil hydraulic characterization

Laboratory soil hydraulic characterization was performed for assessing the soil-water relationships at the SWMPs under study within the period 2021–2023. A total number of 36 undisturbed and disturbed soil samples (including 3 replica per treatment per year) were collected, at a depth of 0–30 cm and at distances of 1 m from the centre of the tree rows, towards the tree inter-rows, each year, and specifically, before (on March, 2021) and after (on October, 2022 and 2023) the application of OM, according to the experimental layout described in Vanella et al. (2025). Note that the results of the main soil physical-chemical main features are reported in Guarrera et al. (2024) and Vanella et al. (2025). In this study, the main soil hydrological characteristics, i.e., the field capacity (FC, at 0.3 bar) and wilting point (WP, at 15 bar) were determined using a Richards' pressure chamber apparatus (Model-1500F2, Soilmoisture equipment corp., Santa Barbara, CA, USA). To compute the volumetric SWC at the FC and WP (cm^3 cm^{-3}), the bulk density (g cm^{-3}) was determined as the ratio between the soil dry weight of each undisturbed soil sample and its volume. Then, the plant available water (PAW, cm^3 cm^{-3}) was estimated as difference between the FC and WP.

A multivariate analyses of variance approach (MANOVAs) was implemented into Statistix software (v.9.0, Analytical Software, Miller Landing Rd Tallahassee, FL) to assess differences on the soil hydrological constants under the adopted SWMPs. More on detail, the influence of three factors, i.e., year (2021, 2022 and 2023); water regime (FI and RDI); and soil management (bare and mulched soils), and their interactions, was analysed on each derived soil hydraulic variable (FC, WP and PAW). The derived significant differences were separated using the *post hoc* Tukey's honest significant difference (HSD) method test with the 95 % of confidence level (p-value < 0.05). Additionally, the inter-annual variability of the soil hydrological variables was analysed by performing independent two-ways and one-way ANOVAs for the periods when geophysical surveys were conducted (2022 and 2023). In particular, the factors analysed at case study 1 were the water regime (FI and RDI) and the soil management (bare and mulched soils), and their interactions; while, the soil management was used as factor for case study 2.

3. Results

3.1. Geophysical monitoring

The results of the ERT surveys are described in the following sub-sections (3.1.1 and 3.1.2) with reference to case study 1 (refer to ERT transects a'-b', c'-d', e'-f', g'-h' in Fig. 1) and case study 2 (refer to ERT transect i'-j' in Fig. 1). The EMI outputs are also depicted in this section with reference to case study 2.

3.1.1. Case study 1

Fig. 3(a) and 3(b) shows the ERT tomograms referring to the ER distribution observed at all the SWMPs of interest (i.e., RDI-Bare, FI-Bare, RDI-Mulch and FI-Mulch, see Section 2.1) at the initial condition (before the beginning of the irrigation cycle, Table 1) during the 2022 irrigation season (July and September).

As expected, on July 2022 (Fig. 3(a)), at the beginning of the irrigation season, higher ER values were observed under both RDI (with average and standard deviation values of 38.15 ± 25.14 Ω m referring to the investigated ERT transects a'-b' and e'-f', respectively) and FI regimes (with average and standard deviation values of 30.49 ± 25.70 Ω m for the ERT transects c'-d' and g'-h', respectively) in bare and mulched soil conditions. Conversely, on September 2022 (Fig. 3(b)), at the end of the irrigation season, a more conductive soil ER distribution was obtained in comparison to the previous period under both bare and mulched soils, resulting in average and standard deviation values of 31.71 ± 13.26 Ω m and 23.53 ± 11.24 Ω m for RDI and FI, respectively.

The highest ER values tended to be concentrated mostly in the middle part of the inter-row areas away from the irrigation lines (150.97 ± 42.80 Ω m), while into the rhizosphere area the ER values tended to remain lower, reaching average minimum ER values of 3.00 ± 0.98 Ω m. This behaviour was in agreement with the higher SWC distribution observed at 0.35 m from the tree trunks and surface drip irrigation lines, being this area directly influenced by irrigation (Fig. 4(a) and 4(b)). Differently, at 0.75 m distance from the tree trunks, the SWC trends were mostly affected by the OM, resulting in higher SWC (up to 36 %) under mulched soils in comparison to the bare conditions (Fig. 4(a) and 4(b)).

As function of depth, site-specific ER can be distinguished at the SWMPs under study, before the beginning of the irrigation event, both on July and September 2022 (Fig. 5). Specifically, more

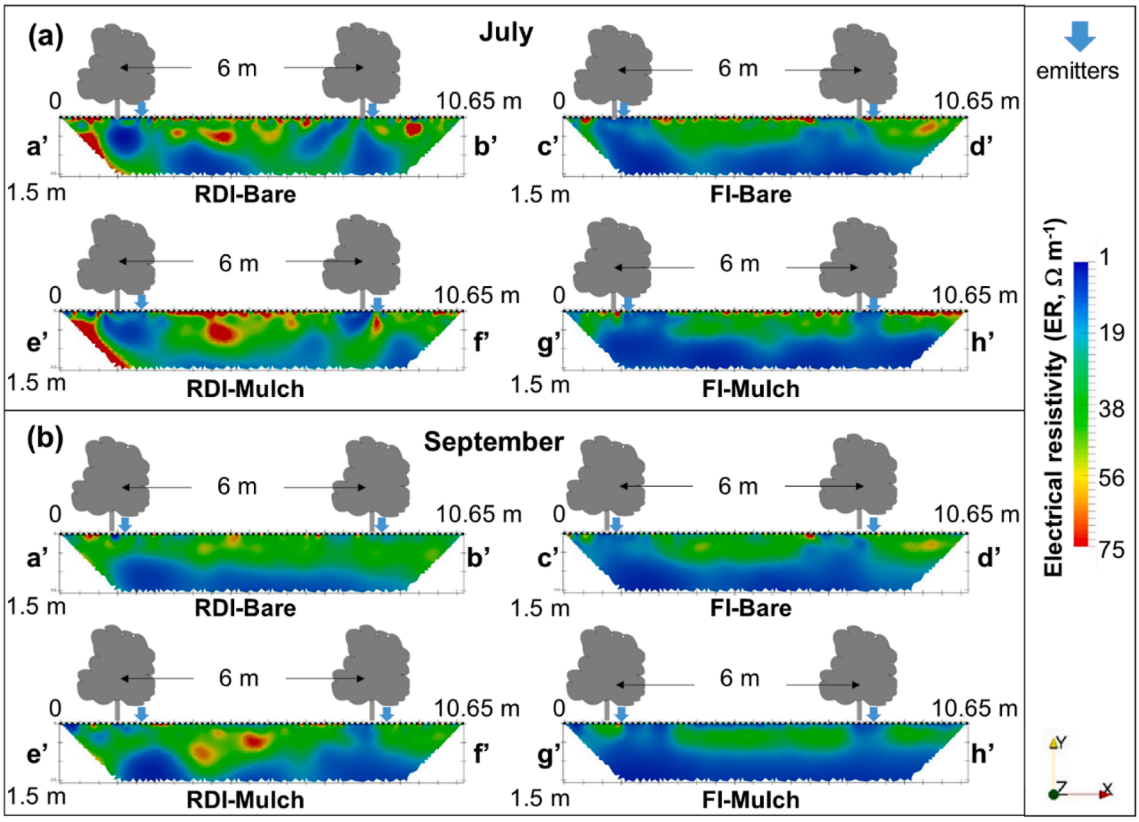

Fig. 3. Two dimensional absolute electrical resistivity (ER) distribution (Ω m) referring to the initial condition, before the beginning of the irrigation phase, on (a) July and (b) September, 2022. ER transects a'-b', c'-d' e'-f' and g'-h' refer the soil water management practices of interest reported in Fig. 1 (see description in Section 2.1).

homogeneous ER conditions were depicted under FI than in RDI regimes during the overall 2022 irrigation season (19.59 ± 2.30 Ω m *versus* 29.15 ± 3.58 Ω m), showing average ER reductions, from July to September, of 12 % and 17 %, respectively, under FI and RDI and of 10 % and 18%, respectively, under bare and mulched soils. Specifically, the Kruskal–Wallis test revealed a significant effect of time on ER (p-value = 0.00), with a higher average values on July (34.32 ± 26 Ω m) than on September (27.62 ± 13.22 Ω m). A strong difference was observed in the first 0.10 m of the soil profile (Fig. 5) between the initial (on July) and the final (on September) part of the 2022 irrigation season, mainly under mulched soils in FI regime, that was characterized by more conductive conditions (up to 68 %); whereas, in bare soils, these differences were limited (up to 32 %). Overall the soil management factor revealed significant differences (p-value = 0.00) between bare and mulch soils, with higher ER values in bare (31.38 ± 18.84 Ω m) than in mulched (30.57 ± 23.04 Ω m) soils. Similarly, the water regime factor revealed marked effect on FI (27.01 ± 20.61 Ω m) compared to RDI (34.93 ± 20.42 Ω m). In the middle part of the investigated soil profile, from 0.20 to 0.90 m of the soil depth (Fig. 5), the averaged ER almost overlapped between July and September, except for RDI-Bare. At the deeper soil layers, above 0.90 m depth (Fig. 5), the average ER showed a sudden reduction largely at the FI regime (with values of 9.74 ± 2.23 Ω m).

The average temporal ER profiles recorded within the short-term monitoring, i.e., during the irrigation phase (from time 0 to time 4 in Table 1), confirmed more homogeneous trends in FI than under RDI water regimes on July, showing overlapping ER profiles as reported in Fig. A1 of the Supplementary material. Analogous ER was obtained also on September under FI, while higher ER anomalies were registered under RDI, resulting in ER changes up to 43 % as showed in Figure A1 (in Supplementary material). The temporal SWC measured by the point-based sensors, located at 0.35 and 0.75 m of distances from the tree trunks to the inter-rows, varied in a narrow range of values with largely constant trends between July (Fig. 3(a) and 0.35 ± 0.01 m^3 m^{-3}) and September 2022 (Fig. 4(b) and 0.32 ± 0.01 m^3 m^{-3}) at the SWMPs under study. As observed in Fig. 4, marked SWC fluctuations were retrieved under RDI conditions in correspondence of the emitters, showing lower initial SWC conditions (0.27 ± 0.04 m^3 m^{-3}) in comparison to the FI regimes (0.38 ± 0.06 m^3 m^{-3}). Conversely, more stable SWC trends were registered under FI (Fig. 3). Moreover, at 0.35 m from the tree trunk, mulched soils resulted in less pronounced SWC fluctuations (Fig. 3(a) and 3(b)). At 0.75 m distance from the tree trunks, the SWC was always higher under mulched soils in comparison to the bare soil conditions (up to 36 %). These observations confirm the higher SWC variability retrieved by ERT under the RDI regimes during the irrigation phase, resulting in more stable SWC under FI, mainly in mulched conditions. The average T_{soil} variations were approximately 2 °C during ERT data acquisition at the SWMPs of interest (Fig. 4(c) and 4(d)).

3.1.2. Case study 2

Fig. 6(a) shows an example of the two-dimensional ER distribution observed under dry conditions on June 2023 at the RDI water strategies under bare and mulched soils, i.e., RDI-Bare and RDI-Mulch (refer to i'-j' ERT transect in Fig. 1), respectively. Specifically, the impact of OM was observed under dry conditions, resulting in lower average (and standard deviation) ER values (p-value = 0.00) under mulched soils (27.18 ± 0.28 Ω m) compared to bare soils (28.04 ± 0.28 Ω m); whereas, ER changes lower than 2 % were observed from the beginning to the end of the ERT survey

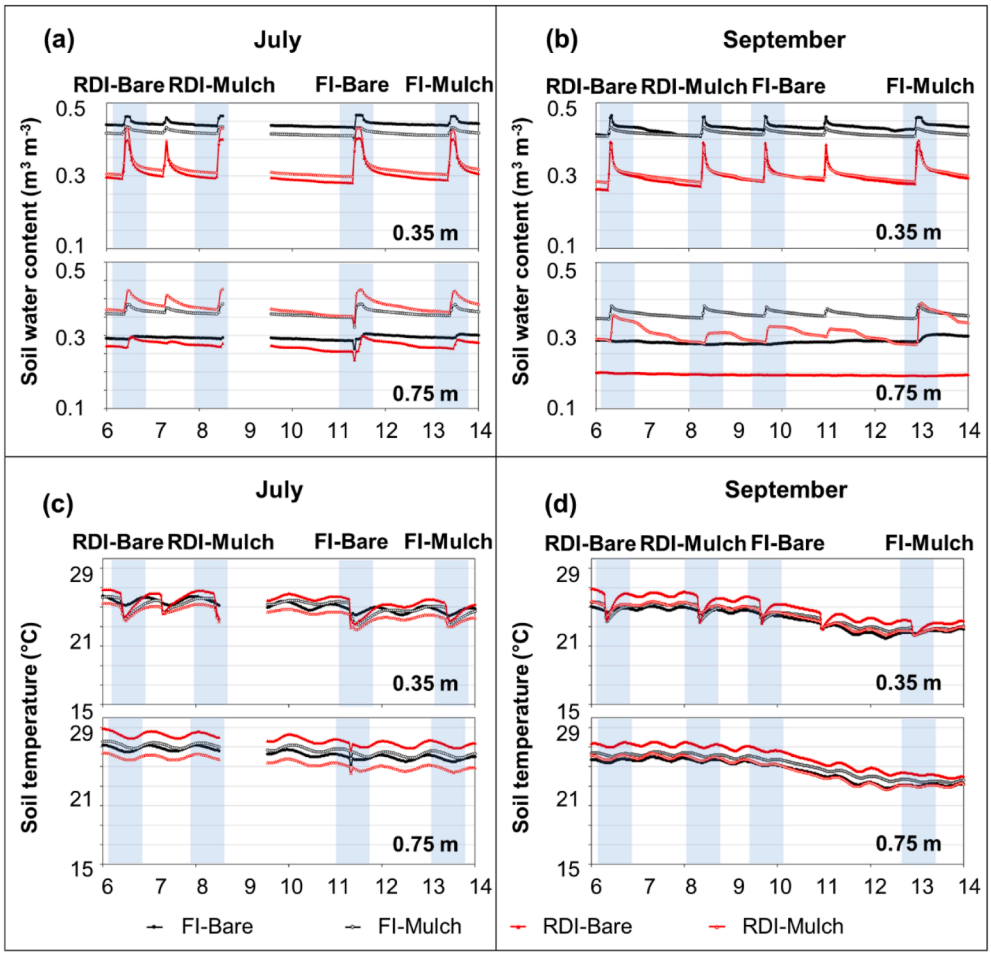

Fig. 4. Hourly temporal soil water content evolution ($m^3\ m^{-3}$), at 0.35 and 0.75 m from the tree trunks to the inter-rows, respectively, observed during the electrical resistivity tomography surveys on (a) July and (b) September 2022; and soil temperature observed at the same distances from the tree trunks on (c) July and (d) September 2022. The terms FI-Mulch, FI-Bare, RDI-Mulch and RDI-Bare refer to the soil water management practices of interest (see description in Section 2.1).

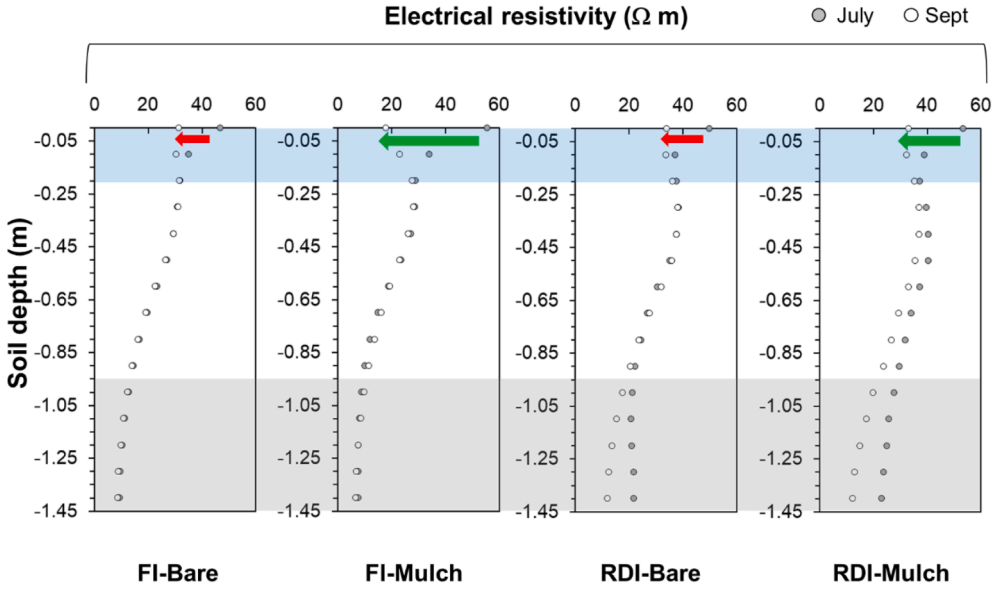

Fig. 5. Average electrical resistivity (ER, Ω m) profiles with depth before the beginning of the irrigation on July and September 2022. The terms FI-Mulch, FI-Bare, RDI-Mulch and RDI-Bare refer to the soil water management practices of interest (see description in Section 2.1).

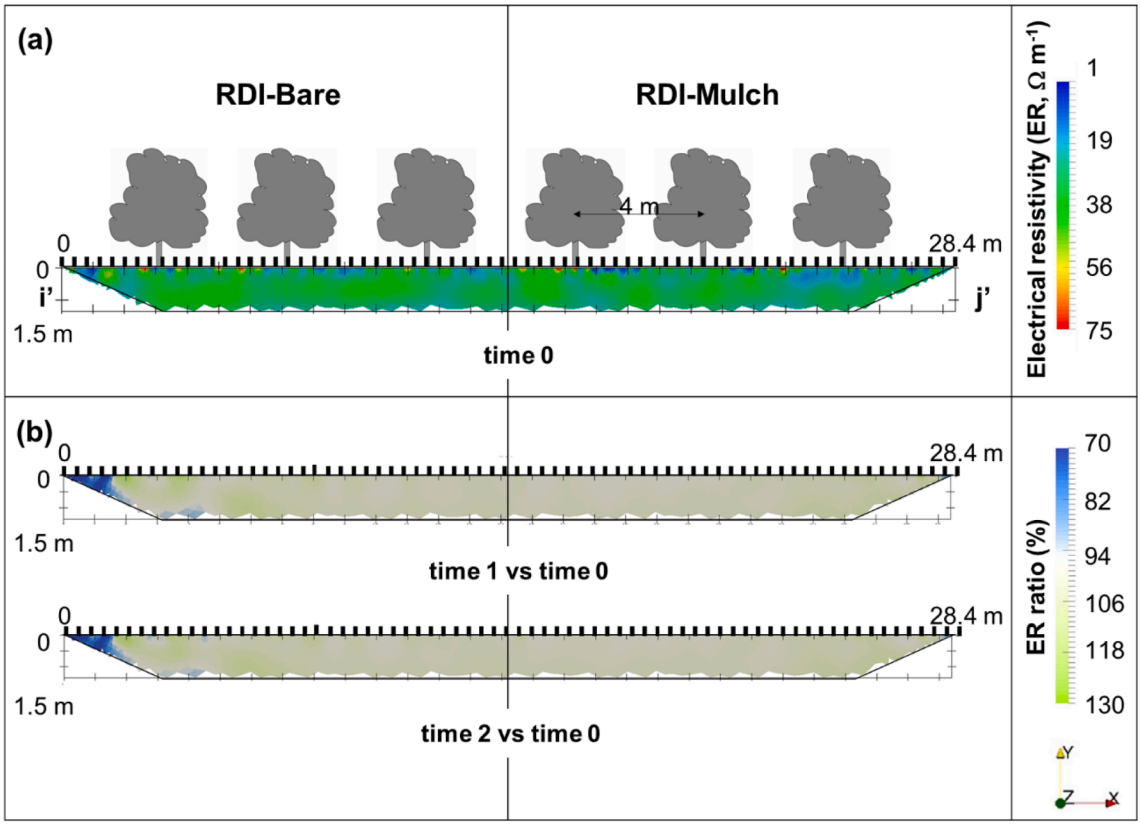

Fig. 6. Example of two-dimensional (a) absolute electrical resistivity (ER) distribution (Ω m); and (b) short-term ER changes observed from time 1 to time 2 on June 29th, 2023 at i'-j' transect under dry conditions (refer to Fig. 1). The terms RDI-Mulch and RDI-Bare refer to the soil water management practices of interest (see description in Section 2.1).

(from time 0 to time 2 in dry conditions, without irrigation application, as reported in Table 2) as confirmed by the outputs of the time-lapse inversion given in Fig. 6(b), which did not show significant relative ER changes (%) respect to the time 0.

The ERT findings in Fig. 6(a) were confirmed by the ECa spatial distribution of the soil subsurface retrieved by EMI, indicating lower ECa values at RDI-Bare compared to RDI-Mulch (Fig. 7(b–c)), and overall homogeneous ECa distribution under the SWMPs at the shallow soil depth (Fig. 7(a)).

Moreover, it is noticeable that overall the ECa increased with depth, resulting in ECa values at 0.5 m of the soil depth (VDP1) ranging from 13 to 17 mS m^{-1} (Fig. 7(a)). The ECa at 1.0 m of the soil depth (VDP2) ranged from 27 to 47 mS m^{-1} (Fig. 7(b)). At the greatest penetration depth (at 1.8 m of the soil depth in Fig. 7(c)), the ECa values increased up to 49 mS m^{-1}. The highest ECa, at all three depth intervals, was found in the middle part of the entire orange orchard; whereas, the lowest ECa values were detected in the Northern-Western side of the plot. The Western sub-area was generally characterised by lower ECa.

The ER distribution in Fig. 8(a) refers to the initial condition, before the beginning of the irrigation, occurred at ERT transect i'-j' (see, Fig. 1) on August 2023. At this temporal stage, lower ER values were obtained in comparison to June 2023 (p-value = 0.00), resulting in similar ER under bare (with average and standard deviation values of 25.31 ± 9.21 Ω m) than mulched soils (with average and standard deviation values of 24.85 ± 8.72 Ω m). From the results of the time-lapse inversions (in Fig. 8(b)), site-specific relative soil wetting and drying patterns can be observed as function of the ER changes under the different explored time-steps in comparison to the initial condition (i.e., time 1–4 *versus* time 0, Table 2), resulting in ER decreases up to 12 % and 14 % under bare and mulched soils, respectively.

The trends showed in Fig. 9, referring to the continuous monitoring of the soil and crop water status variables acquired at case study 2, are in line with the atmospheric water demand, resulting in higher T_{SF} values during the hottest hours of the day within both the explored time periods (June and August 2023, Table 2). In addition, during the ERT surveys, the T_{SF} dynamics were steady, resulting in higher values in bare soil than under mulched soil conditions both on June, with values of 0.05 ± 0.01 mm h^{-1} and 0.03 ± 0.02 mm h^{-1} under bare and mulched soils, respectively; and on August, with values of 0.04 ± 0.02 mm h^{-1} and 0.03 ± 0.02 mm h^{-1} under bare and mulched soils, respectively. Inverse trends of TWP were observed under both the soil management practices under study, resulting in more negative TWP under bare soils (with values of −9.2 ± 0.8 bar) in comparison to mulched soils (with values of −7.9 ± 1.0 bar) on June 2023. Differently, an opposite behaviour was found on August 2023, where more negative TWP values were retrieved under mulched soils (with values of −9.9 ± 0.8 bar) rather than in bare soils (with values of −8.7 ± 0.8 bar). In this latter time period, it is interesting to note that the mulched soils recovered faster their status both in terms of TWP and SWC status (Fig. 9(b)).

The T_{soil} and SWC experienced a constant behaviour during the ERT time-steps on June 2023 at both RDI-Mulch (with average T_{soil} and SWC values of 23.20 ± 0.00 °C and 0.30 ± 0.00 m^3 m^{-3}, respectively) and RDI-Bare (with average T_{soil} and SWC values of 24.80 ± 0.00 °C and 0.29 ± 0.00 m^3 m^{-3}, respectively). Relative abrupt changes were observed on August 2023 both in terms of

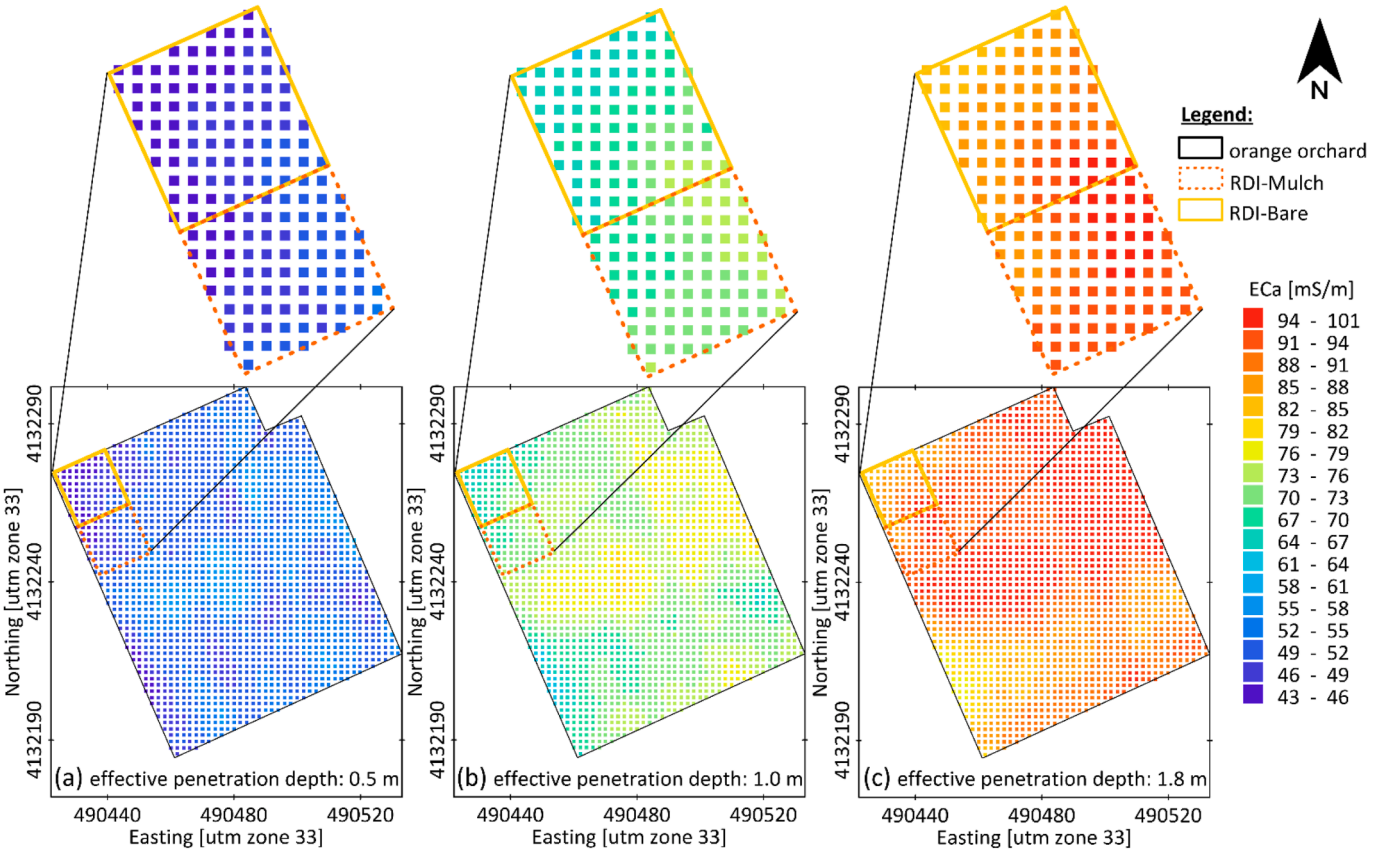

Fig. 7. Apparent electrical conductivity (ECa, mS m^{-1}) distribution of the soil subsurface at dry conditions (no irrigation) on June 29th 2023, with a focus on the regulated deficit irrigation (RDI) regimes, with and without organic mulching (RDI-Mulch and RDI-Bare), using vertical dipole with coil spacing of 0.32 m, 0.71 m, and 1.18 m to achieve effective penetration depths of (a) 0.5 m, (b) 1.0 m, and (c) 1.8 m, respectively. The terms RDI-Mulch and RDI-Bare refer to the soil water management practices of interest (see description in Section 2.1).

T_{soil} and SWC. Specifically, from the beginning to the end of the irrigation event, the semi-hourly SWC values ranged from 0.29 m^3 m^{-3} to 0.40 m^3 m^{-3} and from 0.30 m^3 m^{-3} to 0.40 m^3 m^{-3}, respectively, under bare and mulched soils; whereas, the T_{soil} varied from 24.69 °C to 27.70 °C and from 24.73 °C to 25.30 °C under bare and mulched soils. Note that the SWC and the T_{soil} showed an inverted behaviour as consequence of the irrigation phase occurrence on August 2023 (Fig. 9(b)), in agreement with the findings provided by the time-lapse ERT monitoring (Fig. 8).

3.2. Soil hydraulic characterization

The results of the soil hydraulic characterization, in terms of FC, WP and PAW (cm^3 cm^{-3}), are reported in Table 3 together with the differences obtained for the factors under study.

As reported in Table 3, all the analysed soil hydrological constants showed a time-dependent behaviour, resulting in higher SWC values at the initial condition in 2021, with values of 0.47 ± 0.07 cm^3 cm^{-3}, 0.26 ± 0.05 cm^3 cm^{-3}, 0.21 ± 0.06 cm^3 cm^{-3} for FC, WP and PAW, respectively. Differently, in the period 2022-2023, lower SWC values were observed for FC (with values of 0.40 ± 0.07 cm^3 cm^{-3}) and PAW (with values of 0.10 ± 0.05 cm^3 cm^{-3}), respectively. The WP significantly increased in time, reaching values of 0.29 ± 0.04 cm^3 cm^{-3} and 0.32 ± 0.04 cm^3 cm^{-3} in 2022 and 2023, respectively. Apart of this temporal behaviour, it is interesting to note a clear difference due to the OM application, resulting in higher FC values under mulched soils (with values of 0.43 ± 0.08 cm^3 cm^{-3}) compared to bare soil conditions (with values of 0.41 ± 0.08 cm^3 cm^{-3}). Additionally, significant differences were obtained for the PAW as function of the interaction between water regime and soil management factors, resulting in lower values under RDI in bare soils (with values of 0.12 ± 0.07 cm^3 cm^{-3}) in comparison to RDI in mulched conditions (with values of 0.15 ± 0.08 cm^3 cm^{-3}) for the investigated years; whereas, intermediate PAW values were observed for FI regime (with values of 0.14 ± 0.07 cm^3 cm^{-3}) (Fig. 10).

At case study 1, differences in soil hydraulic parameters were linked to the interaction of soil management and water regime, and, specifically, in 2022, the RDI-Bare exhibited the lowest FC (0.35 ± 0.07 cm^3 cm^{-3}) in comparison to the mulched soils under both RDI (in average 0.40 ± 0.06 cm^3 cm^{-3}) and FI (in average 0.41 ± 0.07 cm^3 cm^{-3}). The WP also showed higher values in mulched plots (0.30 ± 0.04 cm^3 cm^{-3}), and the PAW was greater under FI conditions (0.11 ± 0.06 cm^3 cm^{-3}). At case study 2, some of trends observed at case study 1 were confirmed under RDI, since both FC (0.41 ± 0.06 cm^3 cm^{-3}) and WP (0.31 ± 0.04 cm^3 cm^{-3}) revealed higher values in the presence of mulch.

4. Discussion

The ER distributions obtained at the soil-plant interface reflected the impact of the different irrigation schemes (FI and RDI) and soil management (bare and mulched soils) strategies adopted at case study 1 (i.e., FI-Bare, FI-Mulch, RDI-Bare and RDI-Mulch, Fig. 3) and at case study 2 (i.e., RDI-Bare *versus* RDI-Mulch, Figs. 6 and 8).As expected, the greater ER heterogeneity found

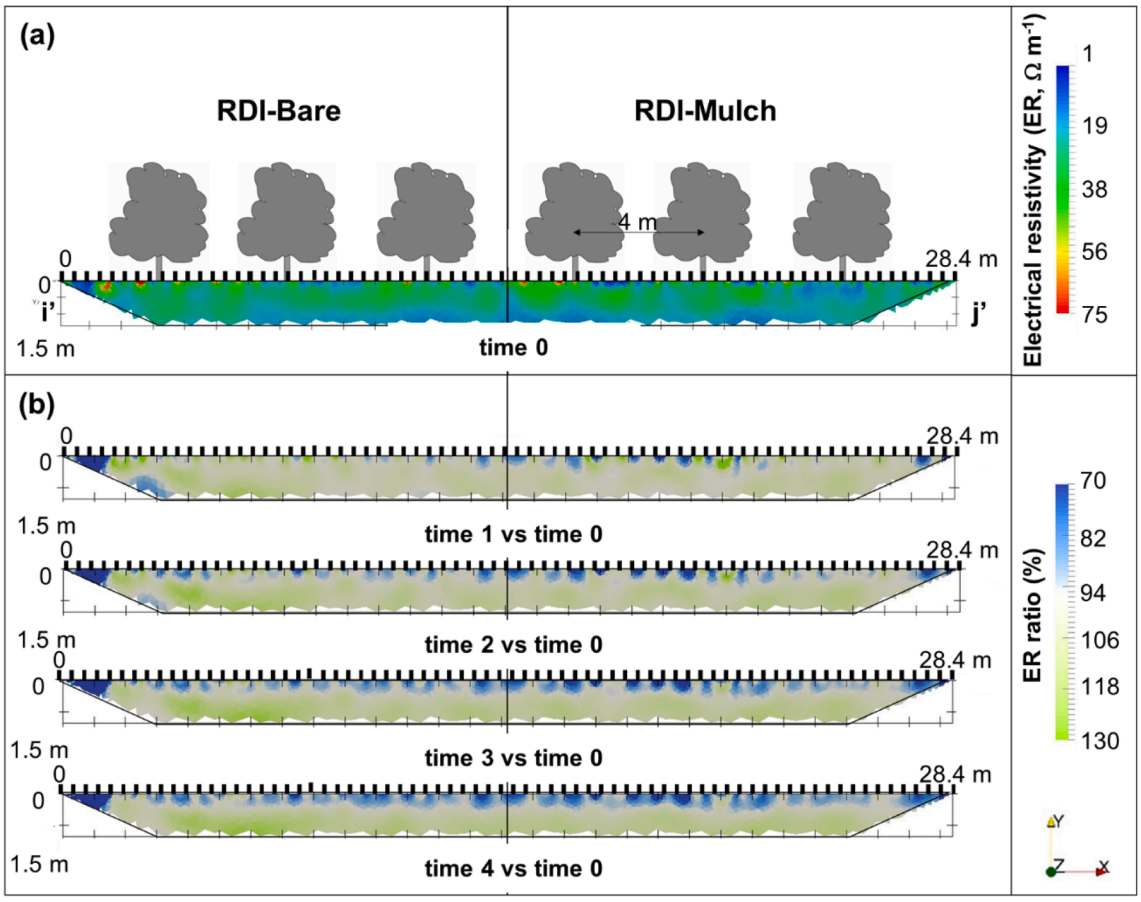

Fig. 8. Two-dimensional absolute electrical resistivity distribution (ER, Ω m) (a) before the beginning of the irrigation (time 0); and (b) short-term ER changes (%) observed within the irrigation phase (from time 1 to time 4) on August 4th, 2023 at i'-j' transect (refer to Fig. 1). The terms RDI-Mulch and RDI-Bare refer to the soil water management practices of interest (see description in Section 2.1).

under the RDI regimes both in bare and mulched soils (Figs. 3 and 5) was confirmed by the local point-based SWC observations that revealed more homogenous SWC under FI regimes (Fig. 4). The lower ER values obtained at FI compared to RDI regimes (Figs. 3 and 5) are in agreement with the findings provided by Vanella et al. (2021). Additionally, the soils under RDI were particularly affected by the irrigation phases at shallow layers (in the 0–35 cm soil profile), mainly under bare soils, at both case studies 1–2 (Figs. 3, 5 and 7). On the contrary, in mulched soils the point-based SWC changes were less pronounced during the irrigation phase (Figs. 4 and 9), showing higher soil water retention and PAW (Table 3 and Fig. 10). These observations are in accordance with Carrera et al. (2022), whose recorded greater SWC variations under conventional soil tillage practices, rather than in conservative soil management treatments. Controversial positive effects of conservative agricultural-practices have been widely reported on soil water availability (Abdallah et al., 2021). These positive effects have been attributed to the increase in water infiltration and reduction in soil evaporation, even though they are limited to the top few centimetres of soil (Minasny & McBratney, 2018). Herein a clear link was identified between the obtained geophysical observations and the application of OM. Both ERT and EMI surveys recognized more conductive areas under the mulched soils both under dry and wet conditions, suggesting higher SWC under these scenarios (Figs. 6 and 7(b) (c), and 8). This behaviour was confirmed during the irrigation events by the SWC observations resulting in higher SWC (up to 36 %) under mulched soils in comparison to the bare soil conditions, at a distance of 0.75 m from the tree trunks to the inter rows, at case study 1 (Fig. 4). The ER patterns detected in the middle of the inter-rows in Fig. 3 were primarily associated to the wetting bulbs expansion that directly influenced the area close to the tree trunks; while, far from the emitters, drier inter-row areas showed higher ER. Similar soil wetting and drier patterns have been observed in Mediterranean irrigated orchards (Vanella et al., 2018, 2021, 2022). Herein, it is interesting to highlight that the use of OM partially increased the SWC in the inter-row areas, thus reducing contrasts in ER (Fig. 3). This finding is supported by Kisekka et al. (2024) that found increased SWC under OM, leading to evident lower ER in the inter-row areas compared to bare soils in almond orchards.

The higher SWC observed under mulched soil (Figs. 4 and 9) highlighted the role of OM in preventing the soil evaporation and improving the soil water retention in accordance to the findings provided by Abdallah et al. (2021). The ER reductions found along the irrigation season (from July to September, 2022) at case study 1 (Fig. 4) can be associated to the higher soil water retention of the OM layer and, thus, to an overall less evaporation rate occurring under the mulched regimes as reported by Liao et al. (2021) in apple orchards under semi-arid climate. Comparable effects have been observed in Mediterranean woody crops. As example, the application of compost and pruning residues in olive groves reduced soil evaporative losses and increased water content (de Sosa et al., 2023; Moreno et al., 2023). Similarly, in citrus orchards, rice-straw mulching and organic amendments enhanced

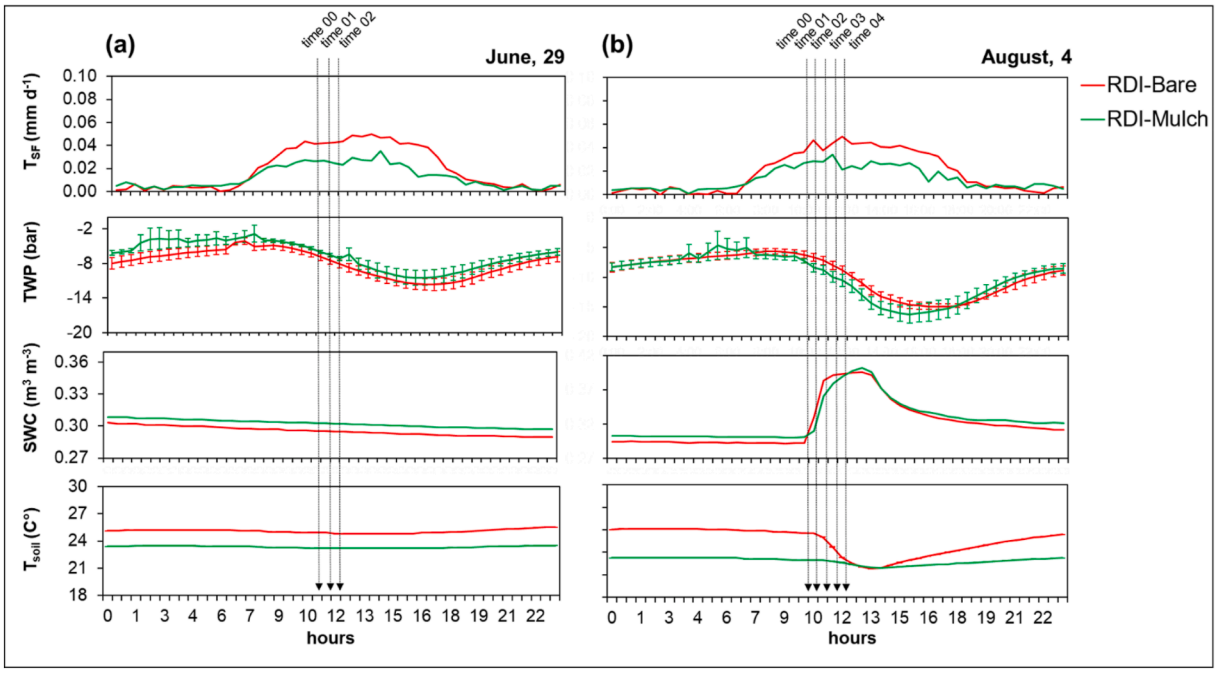

Fig. 9. Evolution of the point-based ancillary variables referring to the soil and tree water status observed at the case study 2 (i.e., transpiration fluxes, trunk water potential, soil water content and soil temperature) on June 29th and August 4th 2023 at the soil management practices under study (bare *versus* mulched soils) in regulated deficit irrigation (RDI) conditions during the time-lapse electrical resistivity surveys. The terms RDI-Mulch and RDI-Bare refer to the soil water management practices of interest (see description in Section 2.1).

Table 3
Average (± standard deviation) values of the soil water content (cm^3 cm^{-3}) referring to the field capacity (FC), wilting point (WP) and plant available water (PAW) for the different factors under study, i.e., year: 2021–2023; water regime: full irrigation (FI) *versus* regulated deficit irrigation (RDI); and soil management: bare *versus* mulched soil. Asterisks indicate the significant differences obtained for the factors under study and their interactions at *p*-value <0.05.

Water regime (WR)	Soil management (SM)	Year	FC (cm^3 cm^{-3})	WP (cm^3 cm^{-3})	PAW (cm^3 cm^{-3})
FI	Bare	2021	0.46 ± 0.06	0.26 ± 0.05	0.20 ± 0.05
	Mulch		0.47 ± 0.07	0.26 ± 0.03	0.21 ± 0.04
RDI	Bare		0.44 ± 0.09	0.26 ± 0.03	0.18 ± 0.07
	Mulch		0.47 ± 0.08	0.24 ± 0.08	0.23 ± 0.06
FI	Bare	2022	0.40 ± 0.08	0.28 ± 0.04	0.12 ± 0.07
	Mulch		0.41 ± 0.07	0.30 ± 0.05	0.11 ± 0.04
RDI	Bare		0.35 ± 0.07	0.27 ± 0.04	0.08 ± 0.04
	Mulch		0.40 ± 0.06	0.30 ± 0.03	0.10 ± 0.04
FI	Bare	2023	0.42 ± 0.06	0.32 ± 0.04	0.10 ± 0.05
	Mulch		0.42 ± 0.06	0.32 ± 0.03	0.10 ± 0.05
RDI	Bare		0.39 ± 0.06	0.30 ± 0.04	0.09 ± 0.03
	Mulch		0.43 ± 0.06	0.33 ± 0.04	0.10 ± 0.04
Factors					
Year			*	*	*
WR					
SM			*		
WR*SM					*
YEAR*WR					
YEAR*SM					
YEAR*WR*SM					

water retention and limited evaporation (Visconti et al., 2024; Hrameche et al., 2024). These outcomes are corroborated by the results of the soil hydraulic characterization, indicating higher FC values under mulched soils (with values of 0.43 ± 0.08 cm^3 cm^{-3}) compared to bare soil conditions (with values of 0.41 ± 0.08 cm^3 cm^{-3}) (Table 3), and in terms of PAW as function of the interaction between water regime and soil management factors, resulting in higher values under the mulched RDI soils (with values of 0.15 ± 0.08 cm^3 cm^{-3}) in comparison to the RDI bare soils (with values of 0.12 ± 0.07 cm^3 cm^{-3}) (Fig. 10). According to other authors, the temporal reduction observed in Table 3 for FC (ranging from 0.47 to 0.40 cm^3 cm^{-3}) and PAW (ranging from 0.21 to 0.10 cm^3 cm^{-3}) can be associated to a gradual degradation of soil structure and decline in soil organic carbon possibly due to soil compaction (Frene et al., 2024; Hamza & Anderson, 2005) and/or OM decomposition (Hudson, 1994; Rawls et al., 2003), being these processes intensified under Mediterranean environments (Zhang et al., 2024). It is interesting to underline the fact that the

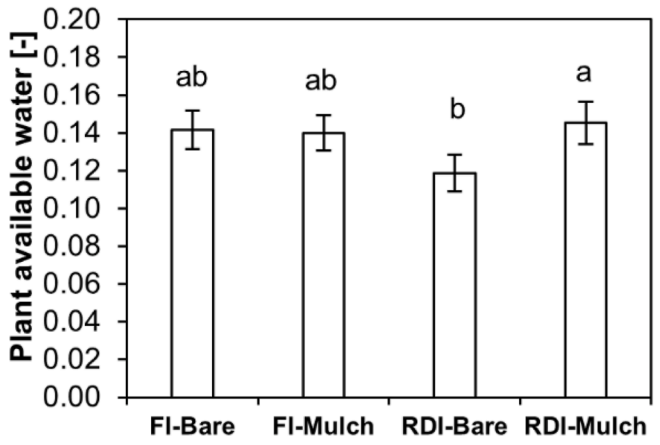

Fig. 10. Interaction of the plant available water (PAW) linked to water regime (full irrigation *versus* regulated deficit irrigation, FI *versus* RDI, respectively) and the soil management (bare *versus* mulched soils) in the three-years period of observation (2021–2023). Bars refer to the standard error associated to the average values. Letters (a, b, ab) show significant differences in accordance with the Tukey test for p-value < 0.05.

interference of climatic factors on soil sampling (i.e., conducted after rain events in 2022, and during drier conditions in 2023; refer to Vanella et al., 2025) did not affect the analysed soil hydraulic parameters, being some of the trends observed at case study 1 confirmed under RDI at case study 2, resulting in higher FC and WP in the presence of OM. However, the effect of OM on SWC involves elucidating mechanisms from multifaceted perspectives, e.g., promoting aggregate formation/stabilization or stimulating microbial activity, that need targeted studies to assess the specific effects of OM on soil pore structure or microbial communities, and their role in water retention.

Site-specific ER variations were denoted with depth among the adopted sustainable SWMPs, indicating the presence of preferential drivers in moisture distribution in the shallow soil layer (0–0.1 m), that led to more conductive patterns under mulched soils at the end of the irrigation season (on September 2022) in comparison to the bare soils (Fig. 5). Above a depth of 0.90 m, ER values collapsed, indicating an increase in SWC (Fig. 5). These findings were in agreement with the EMI observations, that provided larger ECa distribution at greater depths of investigation (Fig. 7(c)) according to the local stratigraphic settings, characterized by alternating layers of marl, clay and limestone of marine origin with high proportions of clay (up to 50 %). In addition, it cannot be excluded that salinity may play a role as well in ECa increasing at the deeper soil layers. A proper joint ERT-EMI inversions may help to solve this issue in future research (von Hebel et al., 2014; Narciso et al., 2025).

As consequence of the irrigation phase, the ER changes were primarily affected by OM, reaching ER increases up to 14 %, at case study 2 (Fig. 8). This resulted in an inverted trend of the SWC and T_{soil} after the irrigation phase (Fig. 9). In contrast, higher T_{SF} rates and more negative TWP values were observed under the organic mulched soils (Fig. 9). As observed at case study 1 (Fig. 4), the SWC response was directly influenced by the irrigation phase in bare soil conditions; whereas, the SWC recovery was faster under the mulched soils suggesting the power of OM to substantially conserve the SWC (Vanella et al., 2025). These findings demonstrated the importance of applying OM in agricultural soils for faster recovering the TWP and SWC status (Fig. 9). According to Kisekka et al. (2024), the TWP tended to became less negative in the afternoon in both soil management (bare *versus* mulched soils), indicating a clear tree water status response to the infiltrated water. These findings contribute to link the soil and crop water status under OM application in RDI and to support the high potential that continuously TWP data has for ecophysiological studies, especially, when combined with additional measurements, including T_{SF} as in this study. However, being our observations limited to the dates of the ERT surveys (Tables 1 and 2), they do not permit to provide complete physiological explanations, (e.g., stomatal regulation and internal hydraulic buffering; Miranda et al., 2022; Rewald et al., 2011), related to root growth and/or OM decomposition, since long-term seasonal information should be taken into account (Blanco & Kalcsits, 2023). Although further research is needed to fully resolve these complex site-specific dynamics, our findings generate testable hypotheses highlighting the buffering role of OM in mediating soil–plant water interactions. Specifically, they suggest that OM can modulate soil infiltration and water redistribution, thereby shaping root-zone water dynamics and ultimately influencing crop water status, potentially leading to temporal lags or partial decoupling (Vaccaro et al., 2025). In this context, targeted physiological studies, integrating long-term monitoring of SWC, T_{soil}, TWP, T_{SF}, and root activity, could provide a direct mechanistic link between soil processes and plant physiological responses under RDI with OM application, establishing a framework to guide sustainable management strategies.

Finally, the results of this study revealed that changes in ER (Figs. 3, 5, 6 and 8) and ECa (Fig. 7) are good *proxies* for inferring the SWC variations over time under the sustainable SWMPs applied at the soil-plant level of the citrus orchard under study. These findings highlight the importance of coupling geophysical surveys with the monitoring of ER-dependent variables and ancillary soil/tree water status measurements (Figs. 4, 9 and 10) for better understanding the soil hydrology-related features and the soil-plant water dynamics of these complex agro-systems, and appraising how trees respond to OM and different water regimes. However, more research is needed for extrapolating these results to larger scales.

5. Conclusion

This study links geophysical observations with SWC variability under sustainable SWMPs (RDI under mulched soils) in Mediterranean citrus groves together with the collection of soil and tree water status data. The results revealed the valuable role of geophysical imaging for tracking the ER dynamics, as *proxy* of SWC changes, under complex agro-systems, highlighting a clear behaviour of mulched soils; while, the EMI results emphasized the homogeneity of the topsoil at the orchard level. The ERT outcomes are in line with the results of the soil hydraulic characterization, indicating higher FC values under mulched soils compared to bare soil conditions, and in terms of PAW as function of the interaction between the water regime and the soil management factors, resulting in higher values under mulched RDI soils in comparison to RDI bare soils.

The study provides practical implications for precision agriculture and water resource management since the adoption of SWMPs contributes to improve key soil-hydrology related processes (i.e., reducing evaporation and enhancing moisture retention), and improve water savings, while maintaining or potentially increasing yield trade-offs for farmers. The combined use of OM and RDI represents a cost-effective strategy also to manage more efficiently citrus groves by recycling the pruning residues in the field and promoting eco-friendly disposal. As practical implication for policymakers, the use of OM allows to align with EU CAP and Green Deal policies promoting soil and water conservation

practices.

However, more research, e.g., repeating measurements during key phenological stages/irrigation levels in multiple soil conditions, is needed to understand the long-term impacts of organic matter on SWC dynamics, and thereby supporting climate-resilient citrus cultivations.

CRediT authorship contribution statement

Daniela Vanella: Writing – review & editing, Writing – original draft, Visualization, Supervision, Methodology, Investigation, Data curation, Conceptualization. **Ulrike Werban:** Investigation, Funding acquisition, Visualization, Writing – review & editing. **Giuseppe Longo-Minnolo:** Investigation, Data curation. **Serena Guarrera:** Investigation, Data curation. **Marco Pohle:** Investigation, Data curation, Visualization. **Simona Consoli:** Investigation, Funding acquisition.

Declaration of competing interest

The authors declare that they have no known competing financial interests or personal relationships that could have appeared to influence the work reported in this paper.

Acknowledgments

This study was carried out within the framework of the projects PRIN 2022 SWAM4Crops "Smart Technologies and Remote Sensing methods to support the sustainable Agriculture WAter Management of Mediterranean woody Crops" (2022SC3CNE), PRIMA 2020 HANDYWATER "Handy tools for sustainable irrigation management in Mediterranean crops", funded by the Italian Ministry of University (PCI2021-121940) and the German Federal Ministry for Education and Research (grant number: 01DH21013A), PRIMA DIONYSUS "Operational adaptation Nexus based systems solutions in Mediterranean Region" (Grant Agreement No 2341), "Approcci Metodologici innovativi a supporto dell'Irrigazione di Precisione – AMIP" (PIAno di inCEntivi per la Ricerca di Ateneo 2020/2022. Linea di Intervento 3 Starting Grant), and "Innovazioni nelle tecniche di osservazione basate su sensori di PROssimità a supporto dell'Agricoltura di Precisione ed applicazioni ambientali – PRO-AP" (PIAno di inCEntivi per la RIcerca di Ateneo 2024/2026". Linea di Intervento 1- Progetti di Ricerca Collaborativa).

In addition, authors wish to thank the researchers and the personnel of Consiglio per la ricerca in agricoltura e l'analisi dell'economia agraria, Centro di Ricerca Olivicoltura, Frutticoltura e Agrumicoltura (CREA-OFA) of Acireale (CT) for their hospitality at the field site; Di Stefano E, Pappalardo S., and Toscano S. for their help during the ERT dataset collection and F. Thomas for help during EMI data collection.

Appendix A. Supplementary data

Supplementary data to this article can be found online at https://doi.org/10.1016/j.iswcr.2026.100660.

References

Abdallah, A. M., Jat, H. S., Choudhary, M., Abdelaty, E. F., Sharma, P. C., & Jat, M. L. (2021). Conservation agriculture effects on soil water holding capacity and water-saving varied with management practices and agroecological conditions: A review. *Agronomy, 11*(9), 1681.

Al-Shammary, A. A. G., Al-Shihmani, L. S. S., Fernández-Gálvez, J., & Caballero-Calvo, A. (2024). Optimizing sustainable agriculture: A comprehensive review of agronomic practices and their impacts on soil attributes. *Journal of Environmental Management, 364*, Article 121487.

Allred, B., Daniels, J. J., & Ehsani, M. R. (2008). *Handbook of agricultural geophysics*. CRC Press.

Araya Vargas, J., Gil, P. M., Meza, F. J., Yáñez, G., Menanno, G., García-Gutiérrez, V., & Sanhueza, J. (2021). Soil electrical resistivity monitoring as a practical tool for evaluating irrigation systems efficiency at the orchard scale: A case study in a vineyard in Central Chile. *Irrigation Science, 39*(1), 123–143.

Becker, S. M., Franz, T. E., Ge, Y., Luck, J. D., & Heeren, D. M. (2025). Geophysical tools for agricultural management: Trends, challenges, and opportunities. *Vadose Zone Journal, 24*(4), Article e70029.

Binley, A. (2015). Tools and techniques: DC electrical methods. In G. Schubert (Ed.), *Treatise on geophysics* (2nd ed.,, *11* (pp. 233–259). Elsevier. https://doi.org/10.1016/B978-0-444-53802-4.00192-5.

Binley, A., & Kemna, A. (2005). DC resistivity and induced polarization methods. In *Hydrogeophysics* (pp. 129–156). Dordrecht: Springer Netherlands.

Binley, A., & Slater, L. (2020). *Resistivity and induced polarization: Theory and applications to the near-surface earth*. Cambridge University Press.

Blanchy, G., Watts, C. W., Richards, J., Bussell, J., Huntenburg, K., Sparkes, D. L., … Binley, A. (2020). Time-lapse geophysical assessment of agricultural practices on soil moisture dynamics. *Vadose Zone Journal, 19*(1), Article e20080.

Blanco, V., & Kalcsits, L. (2023). Long-term validation of continuous measurements of trunk water potential and trunk diameter indicate different diurnal patterns for pear under water limitations. *Agricultural Water Management, 281*, Article 108257.

Brindt, N., Rahav, M., & Wallach, R. (2019). ERT and salinity—a method to determine whether ERT-detected preferential pathways in brackish water-irrigated soils are water-induced or an artifact of salinity. *Journal of Hydrology, 574*, 35–45.

Calamita, G., Perrone, A., Brocca, L., & Straface, S. (2017). Soil electrical resistivity for spatial sampling design, prediction, and uncertainty modeling of soil moisture. *Vadose Zone Journal, 16*(10), 1–14.

Carrera, A., Longo, M., Piccoli, I., Mary, B., Cassiani, G., & Morari, F. (2022). Electromagnetic geophysical dynamics under conservation and conventional farming. *Remote Sensing, 14*(24), 6243.

Cassiani, G., Boaga, J., Vanella, D., Perri, M. T., & Consoli, S. (2015). Monitoring and modelling of soil–plant interactions: The joint use of ERT, sap flow and eddy covariance data to characterize the volume of an orange tree root zone. *Hydrology and Earth System Sciences, 19*(5), 2213–2225.

Chen, B., Garré, S., Liu, H., Yan, C., Liu, E., Gong, D., & Mei, X. (2019). Two-dimensional monitoring of soil water content in fields with plastic mulching using electrical resistivity tomography. *Computers and Electronics in Agriculture, 159*, 84–91.

Consoli, S., Stagno, F., Vanella, D., Boaga, J., Cassiani, G., & Roccuzzo, G. (2017). Partial root-zone drying irrigation in orange orchards: Effects on water use and crop production characteristics. *European Journal of Agronomy, 82*, 190–202.

de Sosa, L. L., Martín-Palomo, M. J., Castro-Valdecantos, P., & Madejón, E. (2023). *Agricultural use of compost under different irrigation strategies in a hedgerow olive grove under*.

European Commission. (2023). *The common agricultural policy 2023–2027*. Brussels: European Commission.

Frene, J. P., Pandey, B. K., & Castrillo, G. (2024). Under pressure: Elucidating soil compaction and its effect on soil functions. *Plant and Soil, 502*(1), 267–278.

Friedman, S. P. (2005). Soil properties influencing apparent electrical conductivity: A review. *Computers and Electronics in Agriculture, 46*(1–3), 45–70.

Garré, S., Hyndman, D., Mary, B., & Werban, U. (2021). Geophysics conquering new territories: The rise of "agrogeophysics". *Vadose Zone Journal, 20*(4), Article e20115.

Geuzaine, C., & Remacle, J. F. (2009). Gmsh: A 3-D finite element mesh generator with built-in pre-and post-processing facilities. *International Journal for Numerical Methods in Engineering, 79*(11), 1309–1331.

Guarrera, S., Vanella, D., Consoli, S., Giudice, G., Toscano, S., Ramírez-Cuesta, J. M., … Longo, D. (2024). Analysis of small-scale soil CO2 fluxes in an orange orchard under irrigation and soil conservative practices. *Heliyon, 10*(9), Article e30543.

Hamza, M. A., & Anderson, W. K. (2005). Soil compaction in cropping systems: A review of the nature, causes and possible solutions. *Soil and Tillage Research, 82*(2), 121–145.

Han, G., & Niles, M. T. (2023). An adoption spectrum for sustainable agriculture practices: A new framework applied to cover crop adoption. *Agricultural Systems, 212*, Article 103771.

Hrameche, O., Tul, S., Manolikaki, I., Digalaki, N., Kaltsa, I., Psarras, G., & Koubouris, G. (2024). Optimizing agroecological measures for climate-resilient olive farming in the mediterranean. *Plants, 13*(6), 900.

Hudson, B. D. (1994). Soil organic matter and available water capacity. *Journal of Soil and Water Conservation, 49*(2), 189–194.

Kisekka, I., Peddinti, S. R., Vanella, D., Andrews, E., Brown, P. H., & Khalsa, S. D. S. (2024). Organic soil amendment effects on soil hydrology in an almond orchard evaluated using time-lapse electrical resistivity tomography. *Agricultural Water Management, 302*, Article 108979.

Liao, Y., Cao, H. X., Liu, X., Li, H. T., Hu, Q. Y., & Xue, W. K. (2021). By increasing infiltration and reducing evaporation, mulching can improve the soil water environment and apple yield of orchards in semiarid areas. *Agricultural Water Management, 253*, Article 106936.

Löbmann, M. T., Maring, L., Prokop, G., Brils, J., Bender, J., Bispo, A., & Helming, K. (2022). Systems knowledge for sustainable soil and land management. *Science of the Total Environment, 822*, Article 153389.

McNeill, J. D. (1980). *Electromagnetic terrain conductivity measurement at low*

induction numbers (Technical Note TN-6). Geonics Ltd.
Minasny, B., & McBratney, A. B. (2018). Limited effect of organic matter on soil available water capacity. *European Journal of Soil Science, 69*(1), 39–47.
Miranda, M. T., Espinoza-Núñez, E., Silva, S. F., Pereira, L., Hayashi, A. H., Boscariol-Camargo, R. L., … Ribeiro, R. V. (2022). Water stress signaling and hydraulic traits in three congeneric citrus species under water deficit. *Plant Science, 319*, Article 111255.
Moreno, M. M., González-Mora, S., Villena, J., & Moreno, C. (2023). Organic hydromulches in young olive trees in pots: Effects on soil and plant parameters. *Agriculture, 13*(12), 2211.
Narciso, J., Verhegge, J., & Van De Vijver, E. (2025). Geostatistical joint inversion of frequency-domain electromagnetic data and direct current resistivity data for near-surface modelling. *Scientific Reports, 15*(1), 36006.
Nijland, W., Van der Meijde, M., Addink, E. A., & De Jong, S. M. (2010). Detection of soil moisture and vegetation water abstraction in a Mediterranean natural area using electrical resistivity tomography. *Catena, 81*(3), 209–216.
Pappalardo, S., Consoli, S., Longo-Minnolo, G., Vanella, D., Longo, D., Guarrera, S., … Ramírez-Cuesta, J. M. (2023). Performance evaluation of a low-cost thermal camera for citrus water status estimation. *Agricultural Water Management, 288*, 108489.
Pathirana, S., Lambot, S., Krishnapillai, M., Cheema, M., Smeaton, C., & Galagedara, L. (2023). Ground-penetrating radar and electromagnetic induction: Challenges and opportunities in agriculture. *Remote Sensing, 15*(11), 2932.
Peruzzo, L., Werban, U., Pohle, M., Pavoni, M., Mary, B., Cassiani, G., … Vanella, D. (2025). High-resolution near-surface electromagnetic mapping for the hydrological modeling of an orange orchard. *EGUsphere, 2025*, 1–33.
Rao, S., Meunier, F., Ehosioke, S., Lesparre, N., Kemna, A., Nguyen, F., … Javaux, M. (2019). Impact of maize roots on soil–root electrical conductivity: A simulation study. *Vadose Zone Journal, 18*(1), Article 190037.
Rawls, W. J., Pachepsky, Y. A., Ritchie, J. C., Sobecki, T. M., & Bloodworth, H. (2003). Effect of soil organic carbon on soil water retention. *Geoderma, 116*(1–2), 61–76.
Regulation (EU) 2021/2115 of the European Parliament and of the Council of 2 December 2021 establishing rules on support for strategic plans to be drawn up by Member States under the Common Agricultural Policy (CAP Strategic plans). *Official Journal of the European Union L, 435*, (2021), 1–186.
Rewald, B., Ephrath, J. E., & Rachmilevitch, S. (2011). A root is a root is a root? Water uptake rates of Citrus root orders. *Plant, Cell and Environment, 34*(1), 33–42.
Romero-Ruiz, A., Garré, S., O'Leary, D., Blanchy, G., & Van De Vijver, E. (2024). *Agriculture and geophysics: Illuminating the subsurface*.
Samouëlian, A., Cousin, I., Tabbagh, A., Bruand, A., & Richard, G. (2005). Electrical resistivity survey in soil science: a review. *Soil and Tillage research, 83*(2), 173–193.
Scudiero, E., Corwin, D. L., Markley, P. T., Pourreza, A., Rounsaville, T., Bughici, T., & Skaggs, T. H. (2024). A system for concurrent on-the-go soil apparent electrical conductivity and gamma-ray sensing in micro-irrigated orchards. *Soil and Tillage Research, 235*, Article 105899.
Slater, L., Binley, A. M., Daily, W., & Johnson, R. (2000). Cross-hole electrical imaging of a controlled saline tracer injection. *Journal of Applied Geophysics, 44*(2–3), 85–102.
Swanson, R. H., & Whitfield, D. W. A. (1981). A numerical analysis of heat pulse velocity theory and practice. *Journal of Experimental Botany, 32*(1), 221–239.
Tso, C. H. M., Kuras, O., & Binley, A. (2019). On the field estimation of moisture content using electrical geophysics: The impact of petrophysical model uncertainty. *Water Resources Research, 55*(8), 7196–7211.
Vaccaro, G., Fusco, M., Alagna, V., Franco, L., Motisi, A., & Iovino, M. (2025). Assessing microtensiometers for monitoring stem water potential in mandarin (Citrus reticulata Blanco) orchard under different irrigation regimes. *Agricultural Water Management, 320*, Article 109873.
Vanella, D., Cassiani, G., Busato, L., Boaga, J., Barbagallo, S., Binley, A., & Consoli, S. (2018). Use of small scale electrical resistivity tomography to identify soil-root interactions during deficit irrigation. *Journal of Hydrology, 556*, 310–324.
Vanella, D., Guarrera, S., Ferlito, F., Longo-Minnolo, G., Milani, M., Pappalardo, G., … Consoli, S. (2025). Effects of organic mulching and regulated deficit irrigation on crop water status, soil and yield features in an orange orchard under Mediterranean climate. *The Science of the Total Environment, 958*, Article 177528.
Vanella, D., Peddinti, S. R., & Kisekka, I. (2022). Unravelling soil water dynamics in almond orchards characterized by soil-heterogeneity using electrical resistivity tomography. *Agricultural Water Management, 269*, Article 107652.
Vanella, D., Ramírez-Cuesta, J. M., Longo-Minnolo, G., Longo, D., D'Emilio, A., & Consoli, S. (2023). Identifying soil-plant interactions in a mixed-age orange orchard using electrical resistivity imaging. *Plant and Soil, 483*(1), 181–197.
Vanella, D., Ramírez-Cuesta, J. M., Sacco, A., Longo-Minnolo, G., Cirelli, G. L., & Consoli, S. (2021). Electrical resistivity imaging for monitoring soil water motion patterns under different drip irrigation scenarios. *Irrigation Science, 39*(1), 145–157.
Visconti, F., Peiró, E., Pesce, S., Balugani, E., Baixauli, C., & de Paz, J. M. (2024). Straw mulching increases soil health in the inter-row of citrus orchards from Mediterranean flat lands. *European Journal of Agronomy, 155*, Article 127115.
von Hebel, C., Rudolph, S., Mester, A., Huisman, J. A., Kumbhar, P., Vereecken, H., & van der Kruk, J. (2014). Three-dimensional imaging of subsurface structural patterns using quantitative large-scale multiconfiguration electromagnetic induction data. *Water Resources Research, 50*, 2732–2748. https://doi.org/10.1002/2013WR014864
von Suchodoletz, H., Pohle, M., Khosravichenar, A., Ulrich, M., Hein, M., Tinapp, C., Schultz, J., Ballasus, H., Veit, U., Ettel, P., Werther, L., Zielhofer, C., & Werban, U. (2022). The fluvial architecture of buried floodplain sediments of the Weiße Elster River (Germany) revealed by a novel method combination of drill cores with two-dimensional and spatially resolved geophysical measurements. *Earth Surface Processes and Landforms, 47*(4), 955–976.
Zhang, B., Jia, Y., Fan, H., Guo, C., Fu, J., Li, S., … Ma, R. (2024). Soil compaction due to agricultural machinery impact: A systematic review. *Land Degradation & Development, 35*(10), 3256–3273.